



Mechanistic insights into chloroacetic acid production from atmospheric multiphase volatile organic compound–chlorine chemistry

Mingxue Li¹, Men Xia^{2,3}, Chunshui Lin^{1,4}, Yifan Jiang¹, Weihang Sun¹, Yurun Wang¹, Yingnan Zhang¹, Maoxia He⁵, and Tao Wang¹

¹Department of Civil and Environmental Engineering, The Hong Kong Polytechnic University, Hong Kong SAR 999077, China

²Institute for Atmospheric and Earth System Research/Physics, Faculty of Science, University of Helsinki, Helsinki 00014, Finland

³Aerosol and Haze Laboratory, Beijing Advanced Innovation Center for Soft Matter Science and Engineering, Beijing University of Chemical Technology, Beijing 100029, China

⁴State Key Laboratory of Loess Science, Institute of Earth Environment, Chinese Academy of Sciences, Xi'an 710061, China

⁵Environment Research Institute, Shandong University, Qingdao 266237, China

Correspondence: Tao Wang (tao.wang@polyu.edu.hk)

Received: 8 October 2024 – Discussion started: 21 October 2024

Revised: 13 January 2025 – Accepted: 26 January 2025 – Published: 31 March 2025

Abstract. Chlorine-containing oxygenated volatile organic compounds (Cl-OVOCs) are indicators of atmospheric chlorine chemistry involving volatile organic compounds (VOCs). However, their formation mechanisms are insufficiently understood. Herein, a strong diel pattern of chloroacetic acid ($C_2H_3O_2Cl$) was observed with daytime peaks at 19 and 13 ppt (1 h averages) in 2020 and 2021, respectively, at a coastal site in southern China. Ethene was previously proposed as the primary precursor responsible for daytime $C_2H_3O_2Cl$ levels, but a photochemical box model based on Master Chemical Mechanism (MCM) simulations indicates that ethene accounts for less than 1 %. Quantum chemical calculations suggest that other alkenes also can act as chloroacetic acid precursors. Using an updated gas-phase VOC–Cl chemistry model, we find that isoprene, the most abundant VOC at the sampling site, along with its oxidation products, accounts for 7 % of the observed $C_2H_3O_2Cl$. Moreover, the simulation with the updated MCM produces appreciable levels of other Cl-OVOCs, especially chloroacetaldehyde, a precursor of $C_2H_3O_2Cl$. We proposed the multiphase reaction of Cl-OVOCs to reconcile the overestimation of Cl-OVOCs and the underestimation of $C_2H_3O_2Cl$ in our gas-phase model. The estimated reactive uptake coefficients for various Cl-OVOCs range from 3.63×10^{-5} to 2.34×10^{-2} , based on quantum chemical calculations and linear relationship modelling. The box model simulation with multiphase chemistry shows that the heterogeneous conversion of chloroacetaldehyde to $C_2H_3O_2Cl$ can contribute 24 %–48 % of the observed levels. Our study thus proposes a formation mechanism of gaseous $C_2H_3O_2Cl$ and highlights the potential importance of multiphase processes in atmospheric organic acid formation.

1 Introduction

Reactive halogen species play an important role in various atmospheric environmental processes, including the depletion of ozone (O_3) in the polar regions, the formation of secondary pollution in polluted areas, and global climate change (Saiz-Lopez et al., 2023; Simpson et al., 2015). Halogen radicals, such as Cl^{\bullet} and Br^{\bullet} , primarily originate from the photolysis of photolabile halogen species and deplete through the reactions with volatile organic compounds (VOCs) and O_3 in the earth's atmosphere (Lawler et al., 2011; Osthoff et al., 2008; Spicer et al., 1998). The chemistry between atmospheric VOCs and reactive chlorine not only facilitates the formation of Cl^{\bullet} -initiated secondary organic aerosols but also promotes the cycling of $\bullet OH-HO_2^{\bullet}-RO_2^{\bullet}$, thereby enhancing the atmospheric oxidation capacity (Choi et al., 2020; Ma et al., 2023; Soni et al., 2023). A deeper understanding of the chemistry between VOCs and Cl^{\bullet} is crucial for enhancing our knowledge of the atmospheric halogen cycle and its environmental impact.

Field measurements have detected several chlorine-containing aldehydes and ketones as indicators of atmospheric chlorine chemistry related to specific VOC species (Le Breton et al., 2018; Masoud et al., 2023). Moreover, ambient levels of halogenated organic acids, including chloro-, bromo-, and iodoacetic acids, have been measured in urban and coastal atmospheres, with ethene suggested as a potential precursor for these compounds (Le Breton et al., 2018; Priestley et al., 2018; Xia et al., 2022; Yu et al., 2019). Chamber experiments examining gas-phase chlorine reactions with specific VOC precursors have identified these chlorine-containing aldehydes and ketones as products, as summarized in Table S1 in the Supplement (Blanco et al., 2010; Canosa-Mas et al., 2001; Kaiser et al., 2010; Orlando et al., 2003; Rodríguez et al., 2012; Wang et al., 2015; Wang and Finlayson-Pitts, 2001; Wennberg et al., 2018). These studies show that chloro-methylbutenone and 4-chloro-crotonaldehyde are distinctive markers for the gas-phase chlorine chemistry of isoprene and butadiene, and inversely, formyl chloride, chloroacetaldehyde, and chloroacetone can be derived from Cl^{\bullet} reactions with various VOC precursors, including isoprene, methyl vinyl ketone (MVK), and methacrolein (MACR). However, chloroacetic acid has not been reported in gas-phase chlorine reaction experiments involving alkenes; instead, it has been proposed that organic acids originate from the ambient multiphase chemistry of aldehydes (Carlton et al., 2007; Franco et al., 2021). The precise generation pathways of these chlorine-containing oxygenated VOCs (Cl-OVOCs), particularly chloroacetic acid, remain unclear.

In this study, field measurements of chloroacetic acid were conducted at a coastal site in Hong Kong during the autumn seasons of 2020 and 2021. The observed chloroacetic acid (as well as bromoacetic acid) was consistently concentrated around midday over the 2 years studied. We aimed to eluci-

date the potential chemical processes leading to chloroacetic acid production by performing quantum chemical (QC) calculations and updated chemical box model simulations, with important implications for understanding the halogen chemistry in the atmosphere.

2 Methods

2.1 Field observations

Two field campaigns were performed from 6 October to 24 November 2020 and from 11 September to 1 November 2021 in a rural area (Cape D'Aguilar; 22.21° N, 114.25° E) on the southeastern tip of Hong Kong Island, China. This site is affected by anthropogenic activities in the nearby urban area and the Pearl River Delta, shipping activities in the nearby waters, biogenic emissions, and long-range transport from eastern China (Peng et al., 2022). Each field campaign simultaneously measured reactive halogens ($C_2H_3O_2Cl$, $C_2H_3O_2Br$, $ClNO_2$, Cl_2 , $HOCl$, $BrCl$, and Br_2), trace gases (NO_x , N_2O_5 , NH_3 , CO , SO_2 , and O_3), aerosol mass concentration ($PM_{2.5}$), aerosol surface area density (S_a), VOCs, NO_2 photolysis frequency (jNO_2), and meteorological parameters (temperature (T) and relative humidity (RH)). Reactive halogens were measured using an iodide-adduct time-of-flight chemical ionization mass spectrometer (I^- -ToF-CIMS, Aerodyne Research). The principles of the I^- -ToF-CIMS have been described in detail (Lee et al., 2014). The reagent ions (I^- and $I(H_2O)^-$) were produced by passing 1 L min^{-1} of CH_3I -containing N_2 air through an inline ionizer (^{210}Po). The peaks of $C_2H_3O_2Cl$, $C_2H_3O_2Br$, $ClNO_2$, Cl_2 , $HOCl$, $BrCl$, Br_2 , N_2O_5 , and $HONO$ were identified via high-resolution peak fitting and verification of the halogen isotopic ratios, according to the natural isotopic abundances of Cl and Br. The mean mass resolution was ~ 4800 . The detection limits were 1.71 ± 1.56 ppt for $C_2H_3O_2Cl$ and 0.31 ± 0.26 ppt for $C_2H_3O_2Br$. The limits were defined as twice the standard deviation in signals observed during background testing. In estimating the mixing ratio of $C_2H_3O_2Br$, the sensitivity ratio of $C_2H_3O_2Br$ to Br_2 was assumed to be the same as that of $C_2H_3O_2Cl$ to Cl_2 . The total uncertainty in the measured chloroacetic acid was estimated to be 11%. Operational details of the CIMS and the measurement of other parameters were given in our previous work (Xia et al., 2022), which reported appreciable levels of reactive bromines for our 2020 campaign.

2.2 Quantum chemical calculations

QC calculations are effective for investigating gas-phase and heterogeneous reaction mechanisms (Ma et al., 2018; Tentscher et al., 2019; Xue et al., 2022) and have been adopted to complement field observations and model simulations (Yang, 2024). In the present study, QC calculations were conducted to explore the Cl^{\bullet} -initiated reaction mech-

Table 1. Model scenarios.

Scenario	Precursor			Uptake of Cl-OVOCs and chloroacetic acid ^a	Heterogeneous formation of chloroacetic acid ^b
	C ₂ H ₄	C ₃ H ₆	C ₅ H ₈		
I	✓				
II		✓			
III			✓		
IV	✓	✓	✓		
V	✓	✓	✓	✓	
VI	✓	✓	✓	✓	✓

^a The reactive uptake of Cl-OVOCs on the aerosols is based on estimated uptake coefficients derived from QC calculations, excluding the heterogeneous formation of chloroacetic acid, and the γ value for chloroacetic acid is assumed to be the same as that for acetic acid (Wang et al., 2020).

^b The yield of chloroacetic acid from the reactive uptake of chloroacetaldehyde is estimated as twice that of oxalic acid from aqueous-phase photochemical reactions involving glyoxal (Carlton et al., 2007).

anisms of alkenes, investigate the multiphase process by which carbonyls convert into organic acids, and predict reactive uptake coefficients (γ) for Cl-OVOCs. The Cl[•] addition of alkenes is a typical barrierless reaction without an available transition state. In determining the reaction characteristics of Cl[•] + alkene reactions, relaxed potential energy surface scans along the dissociation paths of the Cl[•] addition intermediates were conducted to obtain the minimum energy paths; i.e. constrained optimization was performed at each fixed C–Cl distance (Zhang et al., 2020). The structural optimization of Cl[•] addition intermediates and their relaxed scans were performed at the M06-2X/aug-cc-pVTZ level of theory (Zhao and Truhlar, 2008a, b), which has been widely used to study organic chlorine chemistry (Ma et al., 2021; Vijayakumar, 2021).

The key steps of gaseous carbonyl uptake in this work were the solvation of gaseous carbonyls, hydrolysis of aqueous carbonyls, and evaporation of aqueous diols (an inverse reaction of gaseous diol solvation), which are referred to as diol mechanisms (Franco et al., 2021). QC calculations provided the potential energy surface for the above processes. Geometry optimizations and frequency calculations were conducted at the M06-2X/aug-cc-pVTZ level of theory. Gas-phase single-point energies were calculated at the DLPNO-CCSD(T)/aug-cc-pVTZ level of theory with TightPNO and RIJK approximations. Aqueous-phase Gibbs free energies were determined using the thermodynamic cycle method (Marenich et al., 2009; Tentscher et al., 2019), along with solvation free energy at the M06-2X/6-31G(d)//SMD level of theory (Marenich et al., 2009).

Previous computational research has revealed that the solvation and hydrolysis kinetics of a trace gas in microdroplets are related to their reactive uptake coefficients of the trace gas, as observed for N₂O₅ (Fang et al., 2024). We adopted the above reaction energies for the solvation and hydrolysis of several OVOCs and their reported γ values to develop linear relationship models, which can be used to predict the γ values of Cl-OVOCs. All QC calculations were performed us-

ing the Gaussian 16 (Frisch et al., 2019) and ORCA (Neese, 2022) software.

2.3 Box model simulations

The Master Chemical Mechanism (MCM) describes detailed gas-phase degradation mechanisms of VOCs, including H-atom abstraction reactions involving various alkanes and Cl[•] (Jenkin et al., 1997, 2015; Saunders et al., 2003). In our previous studies, we enhanced the original model of gas-phase and heterogeneous chlorine and bromine chemistry by representing the addition reaction products of all alkenes with Cl[•] as a dummy chlorine-containing RO₂[•] radical, except for ethene and propene (Peng et al., 2021; Xia et al., 2022). To investigate the formation mechanism of chloroacetic acid, we refined the gas-phase chlorine chemistry of several key alkenes and incorporated the reactive uptake of Cl-OVOCs into the updated model. The updates included (1) refining the rate constants and branching ratios for Cl[•]-initiated reactions involving typical alkenes; (2) adding the subsequent reaction mechanism of chlorine-containing RO₂[•] radicals, assumed to be the same as the mechanism for the corresponding [•]OH reactions in the MCM; (3) adding the reactive uptake of Cl-OVOCs and chloroacetic acid, whose coefficients for aerosols are estimated from QC calculations or the literature; and (4) adding the heterogeneous production of chloroacetic acid.

All simulations were performed using the Framework for 0-D Atmospheric Modeling (F0AM), version 4.3.0.1 (Wolfe et al., 2016). The model was constrained every 5 min using the diurnal average concentrations of field-observed reactive halogens and relevant species in 2020 (Table S2). A 24 h solar cycle for the campaign-averaged condition was simulated three times to stabilize intermediates, and the results of the last run were used for further analysis. We set up six scenarios (scenarios I–VI in Table 1) to explore the effects of each VOC precursor and the reactive uptake of carbonyls on chloroacetic acid generation.

3 Results and discussion

3.1 Field measurements of chloroacetic acid

The time series of the mixing ratios of $\text{C}_2\text{H}_3\text{O}_2\text{Cl}$ and other meteorological parameters along with the correlation analysis of $\text{C}_2\text{H}_3\text{O}_2\text{Cl}$ concentrations are depicted in Figs. 1 and S1 in the Supplement. Daily averages of pollutant concentrations and meteorological parameters during the two observation periods are listed in Table 2. The mixing ratios of $\text{C}_2\text{H}_3\text{O}_2\text{Cl}$ had a diurnal variation in both observation periods. This variation was similar to the diurnal profiles for Cl_2 , HOCl , BrCl , and Br_2 . The average diurnal peaks for $\text{C}_2\text{H}_3\text{O}_2\text{Cl}$ occurred at midday, with the maximum mixing ratios being 19 ppt in 2020 and 13 ppt in 2021. These values are approximately 5 and 3 times those observed in Manchester, United Kingdom, during winter (Priestley et al., 2018). The levels of $\text{C}_2\text{H}_3\text{O}_2\text{Cl}$ and inorganic reactive chlorine (denoted as Cl_x , where $\text{Cl}_x = 2 \times \text{Cl}_2 + \text{ClNO}_2 + \text{HOCl} + \text{BrCl}$) were higher in 2020 than in 2021.

Correlation analysis from 10:00–14:00 LT (Fig. 1) revealed that the levels of Cl_x had the strongest correlation with the $\text{C}_2\text{H}_3\text{O}_2\text{Cl}$ concentration, with the correlation coefficients being 0.60 and 0.83 in 2020 and 2021, respectively. Daytime S_a and $j\text{NO}_2$ were moderately positively correlated with the $\text{C}_2\text{H}_3\text{O}_2\text{Cl}$ level (Fig. S1), suggesting that aerosols and solar radiation could be involved in $\text{C}_2\text{H}_3\text{O}_2\text{Cl}$ formation. Previous studies have revealed that nitrate photolysis on aerosols is an important source of atmospheric Cl_2 and Br_2 at the study site (Peng et al., 2022; Xia et al., 2022). We thus hypothesize that chloroacetic acid can be derived from photochemical processes relating to aerosols. The negative correlation between $\text{C}_2\text{H}_3\text{O}_2\text{Cl}$ and RH may be related to the removal of $\text{C}_2\text{H}_3\text{O}_2\text{Cl}$, such as reactive uptake onto clouds or aerosols.

3.2 Gas-phase chlorine chemistry of alkenes

The original MCM incorporates the formation mechanisms of chloroacetic acid with 1-chloroethane, 1,2-dichloroethane, and 1,2-dichloropropane as precursors. The specific mechanisms are depicted in Fig. S2 in the Supplement. First, 1-chloroethane and 1,2-dichloroethane are oxidized by $\cdot\text{OH}$ to produce chloroacetaldehyde, and 1,2-dichloropropane is oxidized to form chloroacetone. Subsequently, chloroacetic acid as a second-generation product is generated through the $\cdot\text{OH}$ oxidation of chloroacetaldehyde and photolysis of chloroacetone. However, to our knowledge, these three halocarbons have not been detected in field observations conducted in Hong Kong (Cao et al., 2023; Zeng et al., 2020).

Ethene has been proposed as a precursor of chloroacetic acid (Priestley et al., 2018) and was included in our previous work as part of the original model (Xue et al., 2015). However, simulation based on the original model shows that the ethene + Cl^\bullet reaction yields only 0.1 ppt of chloroacetic acid

(< 1 % of the observed value) while producing a higher concentration of Cl-OVOCs, mainly containing chloroacetaldehyde (at a maximum of 43 ppt), as plotted in Fig. S3.

To explain the observed elevated concentrations of chloroacetic acid, we propose gas-phase chlorine chemistry from alternative precursors to modify the original model, now referred to as the updated model. Due to differences in the reaction rate constants and branching ratios for each pathway involving alkenes and Cl^\bullet (NIST Chemical Kinetics Database, 2024), we performed QC calculations to reveal their reaction patterns through potential energy surface scans, as depicted in Figs. 2 and S4–S6. For propene, Cl^\bullet preferentially adds to the terminal C (α -C) rather than the middle C (β -C). The α -C addition intermediate (IM1) of propene is lower in energy than the β -C addition intermediate (IM2), and IM2 spontaneously converts to IM1 by overcoming a low energy barrier ($\sim 8 \text{ kcal mol}^{-1}$), as shown in Fig. 2. Isoprene, MVK, and MACR exhibit similar patterns (Figs. S3–S5). Our QC calculations indicate that α -C addition is the primary pathway for the alkene + Cl^\bullet reactions, with negligible β -C addition. In contrast, previous chemical models only incorporate detailed reaction mechanisms for propene and Cl^\bullet (including α -C and β -C addition) and rough mechanisms for other alkenes (Xue et al., 2015).

Based on the above QC calculations, we refined the Cl^\bullet -initiated reaction rate constants and branching ratios of alkenes (Table S3) and updated the gas-phase chlorine chemistry of several alkenes, as summarized in Fig. 3 (with the details for propene, isoprene, MVK, and MACR presented in Figs. S7–S10). The updated gas-phase mechanism reveals that chloroacetaldehyde and chloroacetone are first-generation products of other alkenes, excluding ethene, whereas chloroacetic acid serves as a second-generation product of these compounds. In particular, chloroacetaldehyde and chloroacetone have been identified as ubiquitous products of gas-phase chlorine reactions of alkenes, such as isoprene, MVK, and MACR, in chamber experiments (Table S1). Additionally, propene is proposed as a precursor to chloroacetone (Wang et al., 2023).

We next investigated the contribution of several typical alkenes to chloroacetic acid using the updated gas-phase mechanism. The simulation is described as scenarios II–IV in the Methods section. The results show that adding gas-phase formation pathways of chloroacetic acid in our updated model accounts for 8 % of the observed mixing ratio, and isoprene and its oxidation products play a major role (Fig. S3). The low yield of chloroacetic acid is explained as follows. The degradation of chloroacetaldehyde is primarily driven by H-atom abstraction from the aldehyde group, leading to the formation of the acyl peroxy radical $\text{CH}_2\text{CICO}_3^\bullet$. However, only a small fraction of $\text{CH}_2\text{CICO}_3^\bullet$ is converted to chloroacetic acid through reactions with HO_2^\bullet and RO_2^\bullet , whereas the majority of $\text{CH}_2\text{CICO}_3^\bullet$ reacts with NO to form $\text{CH}_2\text{ClO}_2^\bullet$. The contribution of chloroacetone to $\text{CH}_2\text{CICO}_3^\bullet$

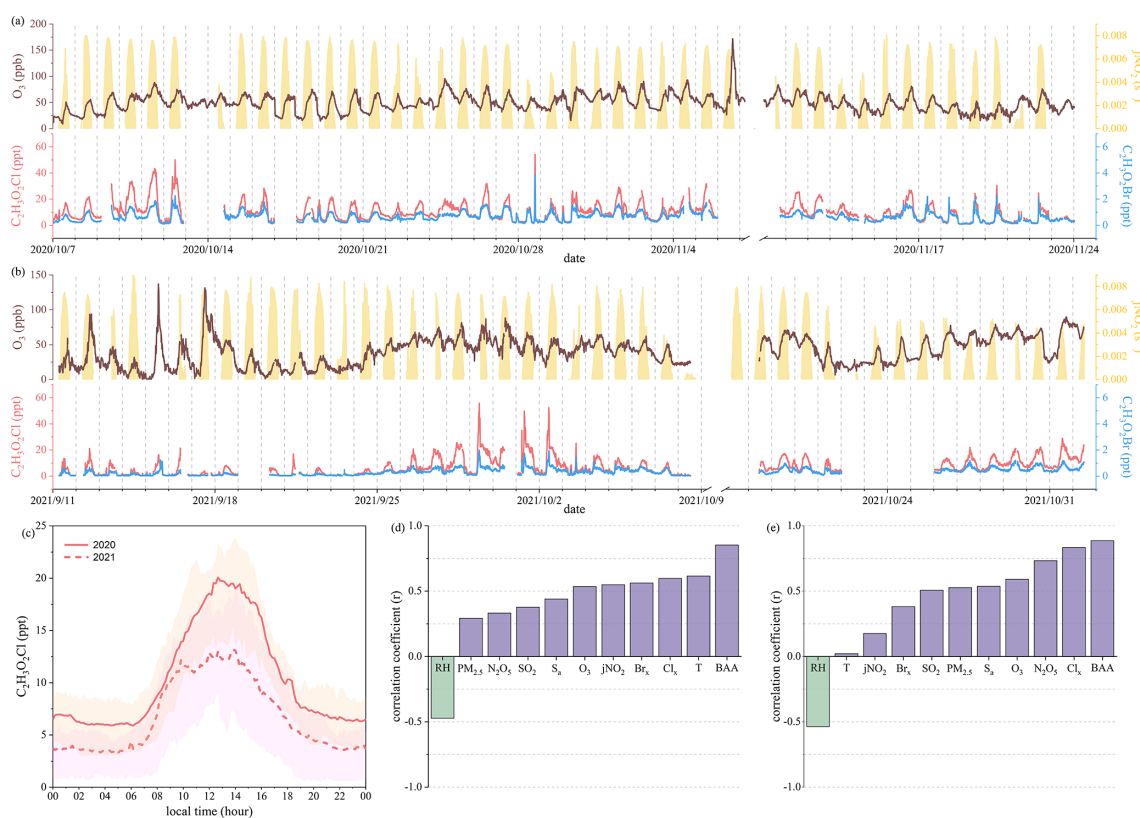


Figure 1. Field observations of chloroacetic acid ($\text{C}_2\text{H}_3\text{O}_2\text{Cl}$) at a coastal site. **(a, b)** Time series of the mixing ratios of O_3 , $j\text{NO}_2$, $\text{C}_2\text{H}_3\text{O}_2\text{Cl}$, and $\text{C}_2\text{H}_3\text{O}_2\text{Br}$ (denoted as BAA) in **(a)** 2020 and **(b)** 2021. **(c)** Average diurnal variations in $\text{C}_2\text{H}_3\text{O}_2\text{Cl}$ in 2020 and 2021. The shaded areas represent 25 %–75 % of $\text{C}_2\text{H}_3\text{O}_2\text{Cl}$. **(c, d)** Coefficients of correlation between $\text{C}_2\text{H}_3\text{O}_2\text{Cl}$, meteorological factors, and chemical constituents from 10:00–14:00 LT in **(d)** 2020 and **(e)** 2021. $\text{Cl}_x = 2 \times \text{Cl}_2 + \text{ClNO}_2 + \text{HOCl} + \text{BrCl}$. Data are 10 min averages in **(a)** and **(c)** and 1 h averages in **(d)** and **(e)**. Please note that the date format used in this figure is year/month/day.

Table 2. Daily average values of pollutant concentrations and meteorological parameters.

Parameter	2020	2021	Parameter	2020	2021
RH (%)	75.0 ± 11.0	81.1 ± 8.2	ClNO_2 (ppt) ^b	491.2 ± 388.1	173.4 ± 171.4
T ($^\circ\text{C}$)	24.0 ± 1.8	27.2 ± 3.2	Cl_2 (ppt)	15.4 ± 16.4	11.5 ± 13.9
$j\text{NO}_2$ (10^{-3} s^{-1}) ^a	6.2 ± 1.8	5.3 ± 2.4	HOCl (ppt)	38.3 ± 26.0	31.5 ± 35.9
S_a ($\mu\text{m}^2 \text{ cm}^{-3}$)	178.5 ± 81.9	103.6 ± 65.2	BrCl (ppt)	0.62 ± 0.56	0.36 ± 0.35
$\text{PM}_{2.5}$ ($\mu\text{g m}^{-3}$)	17.5 ± 7.4	8.8 ± 6.3	Br_2 (ppt)	3.0 ± 1.9	1.1 ± 1.1
SO_2 (ppb)	2.7 ± 1.0	5.1 ± 0.5	$\text{C}_2\text{H}_3\text{O}_2\text{Cl}$ (ppt)	10.1 ± 6.9	6.9 ± 6.5
O_3 (ppb)	49.6 ± 16.5	40.6 ± 20.2	$\text{C}_2\text{H}_3\text{O}_2\text{Br}$ (ppt)	0.65 ± 0.36	0.34 ± 0.26

^a The 1 h average at midday. ^b Average value at night (18:00–05:00 LT next day).

is considered negligible because of its low photolysis rate constant in the MCM.

Our gas-phase VOC–Cl model predicts the generation of up to 1 ppb of Cl-OVOCs (Fig. 4). Reactions of isoprene and its oxidation products (MVK and MACR) with Cl^\bullet account for $\sim 91\%$ of Cl-OVOCs, and others from ethene and propene play a minor role. Formyl chloride is the most abundant Cl-OVOC predicted by the model, followed by chloroacetaldehyde and finally chloroacetone. All three Cl-

OVOCs were identified in previous field observations of reactive chlorine species (Le Breton et al., 2018), but their concentrations were far lower than the levels predicted using our model.

Our updated gas-phase alkene + Cl^\bullet reactions explain only 8 % of the observed chloroacetic acid concentration and significantly overestimate Cl-OVOCs. The photochemical formation of chloroacetic acid and Cl-OVOCs results in their simulated diurnal cycles of daytime increase and night-

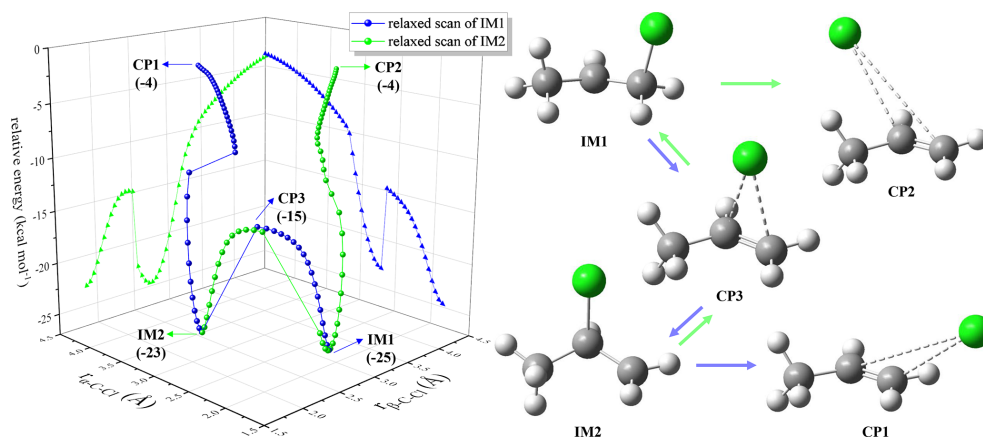


Figure 2. Relaxed scan of the dissociation of Cl^* and propene (C_3H_6) addition intermediates. IM1 and IM2 are intermediates for Cl^* addition to α -C and β -C of propene, and CP1, CP2, and CP3 are the complexes derived from scans of IM1 and IM2 in terms of bond lengths (r) of α -C–Cl and β -C–Cl as variables, respectively. Scanned potential energy surfaces of IM1 (in blue) and IM2 (in green) take the total energy of the reactants $\text{Cl}^* + \text{propene}$ as zero for reference. Energy in brackets in kcal mol^{-1} .

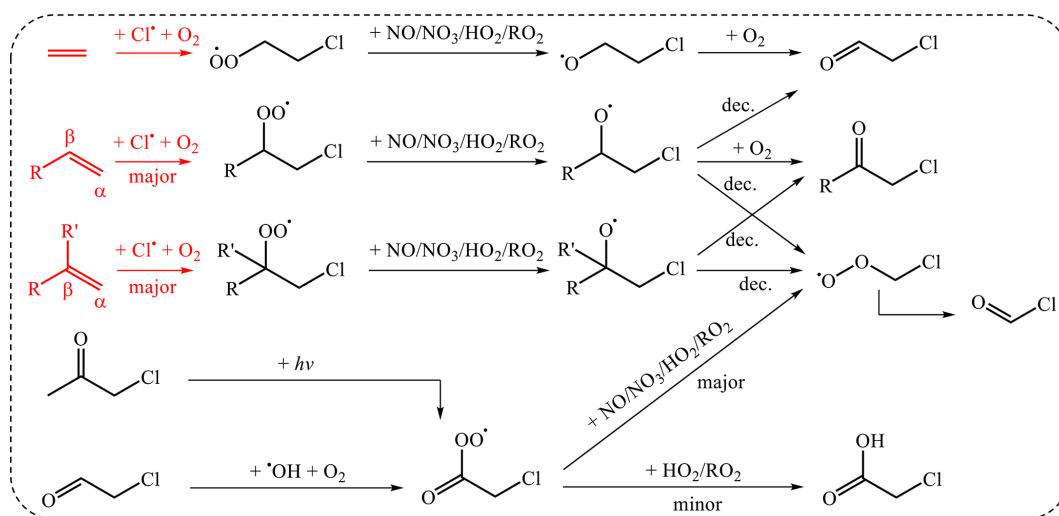


Figure 3. Gas-phase chlorine chemistry of typical alkenes. The MCM outlines the gas-phase generation of carbonyls, shown in black, and the Cl^* -initiated reactions of alkenes are illustrated according to QC calculations in red. R and R' denote substituents. Decomposition: dec.

time decrease, failing to replicate the observed patterns. The inconsistency between simulated and observed results of chloroacetic acid and Cl-OVOCs implies possible missing sinks or sources. Previous studies have reported that reactive uptake coefficients (γ) of several OVOCs (e.g. formaldehyde, glyoxal, methylglyoxal, acetone, 2-butanone, 2,3-butanedione, and acetic acid) onto water or aerosol surfaces can reach levels of $10^{-5} - 10^{-3}$ (De Haan et al., 2018; Iraci and Tolbert, 1997; Liggió et al., 2005; Schütze and Herrmann, 2004; Wang et al., 2020). Proposed multiphase mechanisms of the conversion of aldehydes to gaseous organic acids involve the multiphase equilibrium of aldehydes, diols, and acids; aldehyde hydrolysis; and gas- and aqueous-phase $^{\bullet}\text{OH}$ oxidations of diols, and they explain the production of formic acid from formaldehyde (Franco et al., 2021). More-

over, previous research has revealed heterogeneous reactions as an important source of formic acid (Jiang et al., 2023). We thus propose the reactive uptake of chloroacetic acid and Cl-OVOCs and heterogeneous production of chloroacetic acid, and we estimate the contribution of multiphase processes to the formation of gaseous chloroacetic acid.

3.3 Multiphase production of chloroacetic acid

To address the overestimation of the chloroacetaldehyde level and the underestimation of the chloroacetic acid level in our gas-phase chlorine model, we propose multiphase conversion mechanisms of chloroacetaldehyde to gaseous chloroacetic acid and conducted QC calculations to determine the reaction potential energy surface (Fig. 5). Gaseous

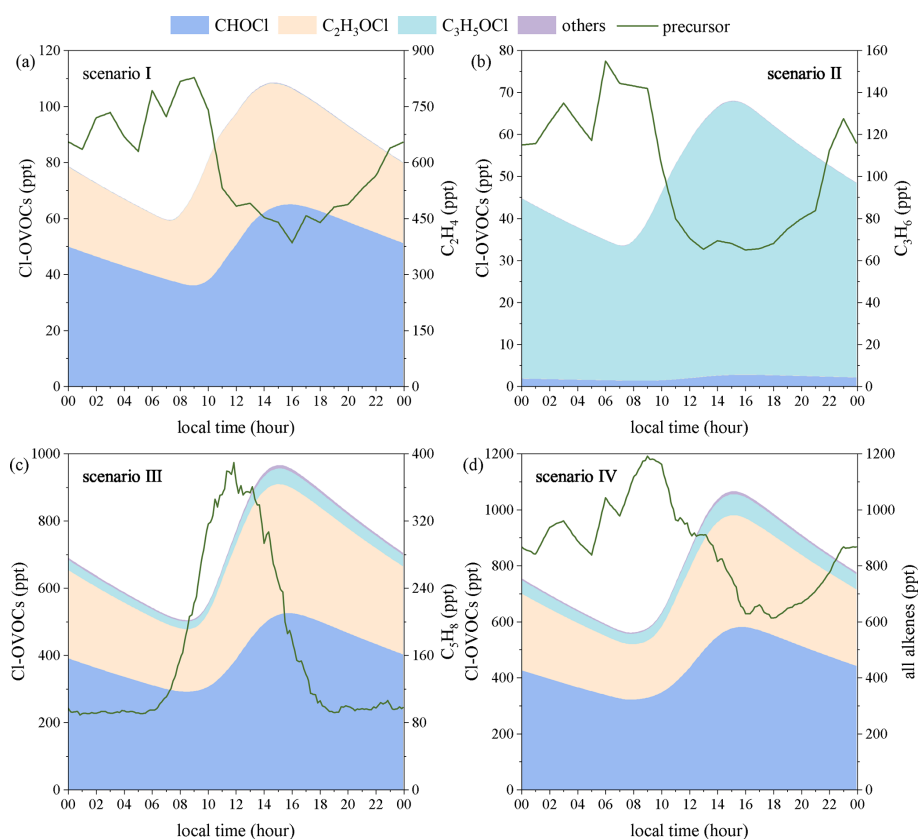


Figure 4. Box-model-simulated diurnal profiles of Cl-OVOCs generated from gas-phase VOC + Cl^{*} reactions: profiles for (a–c) ethene, propene, and isoprene, respectively, and (d) all alkenes (the sum of three alkenes). The diurnal profiles of C₂H₃O₂Cl (maximum of 1.6 ppt) are not visible. Scenarios I–IV are described in Table 1.

chloroacetaldehyde could dissolve in the atmospheric condensed phase, and aqueous chloroacetaldehyde then hydrates to form chloral hydrate. Finally, the diol could react with ^{*}OH to form chloroacetic acid. The calculated energy barrier of chloroacetaldehyde hydrolysis with a water molecule reaches 37.5 kcal mol⁻¹, which is reduced by the water dimer and trimer to 25.2 and 21.3 kcal mol⁻¹, respectively. Considering the acidic nature of aerosol, a molecule of sulfuric acid catalyses chloroacetaldehyde hydrolysis with an energy barrier of 6.1 kcal mol⁻¹. Multiple water molecules or acid catalysts involved in the hydrolysis reaction significantly lower the energy barrier, indicating the rapid hydrolysis feasibility of chloroacetaldehyde in atmospheric aerosols. QC calculations also indicate that chloroacetic acid readily forms from chloral hydrate undergoing ^{*}OH oxidation and O₂ abstraction due to the low energy barriers in both gas and aqueous phases, as depicted in Fig. 5b. The QC calculations support the plausibility of the multiphase formation of chloroacetic acid.

To aid atmospheric models in simulating multiphase reactions of Cl-OVOCs, we conducted QC calculations to determine the γ values for chloroacetaldehyde and other Cl-OVOCs, including formyl chloride and chloroacetone (see

the Methods section). Briefly, we established linear relationships between the QC-calculated multiphase reaction energy and γ reported in previous experimental studies for several OVOCs, and we then used the derived relationships to predict the γ values of Cl-OVOCs. Note that we assume that gas-phase diffusion limitations of OVOCs were negligible, given their low uptake coefficients. The model $\lg \gamma = -2.796 - 0.154\Delta_r G_{\text{hyd}}$ has the largest correlation coefficient (R^2) of 0.727, lowest residual sum of squares (RSS) of 0.550, and smallest standard deviation (SD) of 0.371, where $\Delta_r G_{\text{hyd}}$ is the change in Gibbs free energy for mono-hydration reactions (Fig. S11). The γ values predicted for formyl chloride, chloroacetaldehyde, and chloroacetone are 2.34×10^{-2} , 8.23×10^{-4} , and 7.07×10^{-5} , respectively. The predictions for the other Cl-OVOCs are given in Table S4.

We then added the reactive uptake of Cl-OVOCs on ambient aerosol surfaces in our updated MCM model using λ determined in the above QC calculations. As shown in Fig. 6, the reactive uptake of Cl-OVOCs on aerosol surfaces reduces the maximum Cl-OVOC concentration from the level of parts per billion (ppb) to 64 ppt, contributing to a chloroacetaldehyde loss of up to 92 % in our box model simulation. The reactive uptake of Cl-OVOCs serves as an important sink

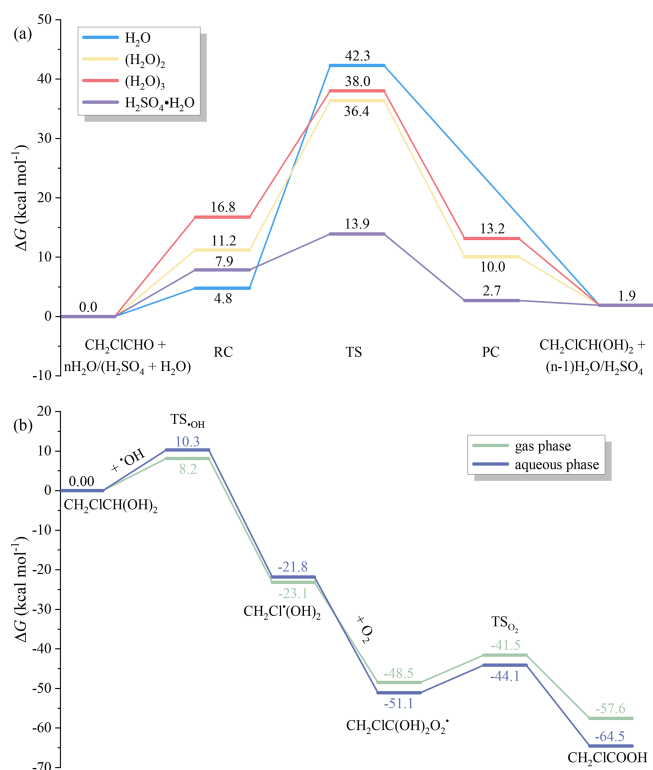


Figure 5. QC-calculated potential energy surfaces of multiphase conversion of chloroacetic acid from chloroacetaldehyde at 298 K. **(a)** Hydrolysis potential energy surfaces of chloroacetaldehyde with water monomer (H₂O), water dimer ((H₂O)₂), water trimer ((H₂O)₃), and sulfuric acid (H₂SO₄) in aqueous phase; **(b)** potential energy surfaces of the conversion of chloral hydrate to chloroacetic acid in gas and aqueous phases. TS denotes the transition state connecting reactants and products; RC and PC denote reactant complex and product complex. ΔG : Gibbs free energy difference of reactions.

for Cl-OVOCs and would resolve the overestimation of Cl-OVOC levels by our gas-phase model.

The proposed multiphase conversion mechanisms of chloroacetaldehyde to chloroacetic acid are depicted in Fig. 7. They can be simplified as $\text{CH}_2\text{ClCHO}(\text{g}) + \text{H}_2\text{O}(\text{l}) \rightarrow \text{CH}_2\text{ClCOOH}(\text{g}) + \text{other products}$. The first-order loss rate of chloroacetaldehyde on aerosols is calculated using the γ value estimated above. To assess the contribution of heterogeneous processes to chloroacetic acid formation, we estimated the yield (φ) of chloroacetic acid from chloroacetaldehyde uptake as follows. A previous laboratory study shows a yield of 1 %–2 % for oxalic acid from aqueous-phase photochemical reactions of glyoxal (Carlton et al., 2007). We assumed the yield (φ) of chloroacetic acid from chloroacetaldehyde is twice the above process because the heterogeneous production of chloroacetic acid involves one diol reaction, whereas that of oxalic acid undergoes two diol reactions.

As discussed in Sect. 3.2, the gas-phase chlorine chemistry of alkenes accounts for only 8 % of the observed chloroacetic

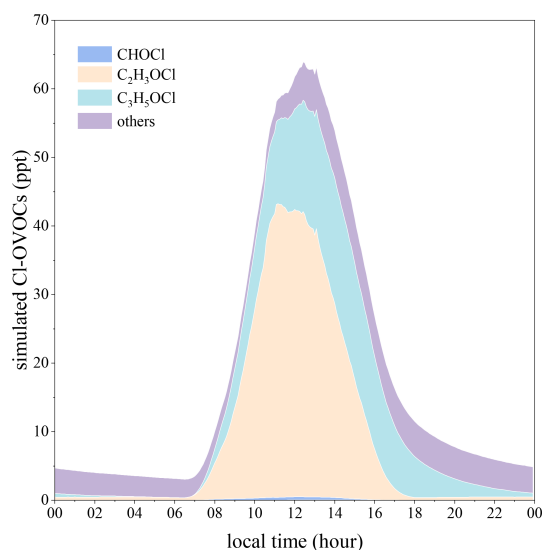


Figure 6. Box-model-simulated diurnal profiles of Cl-OVOCs generated from VOC + Cl* reactions with Cl-OVOC and chloroacetic acid uptake on an aerosol surface (scenario V in Table 1).

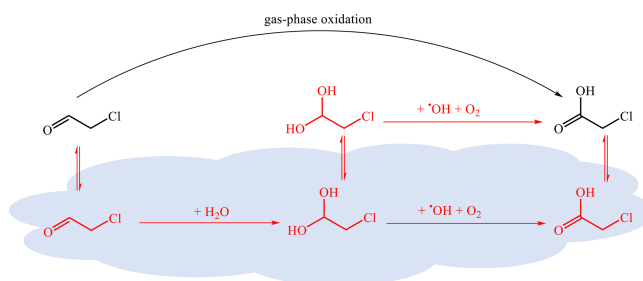


Figure 7. Multiphase production of chloroacetic acid. The gas-phase conversion of chloroacetaldehyde to chloroacetic acid, shown in black, is described in Fig. 3, whereas the multiphase reactions in red are presented in Fig. 5 according to QC calculations.

acid level and fails to explain the observed diurnal cycle. Adding the reactive uptake of chloroacetic acid on aerosols aligns the simulated and observed daily variation, and including the heterogeneous source of chloroacetic acid increases the simulated level to 24 %–48 % of the observed level (Fig. 8). A sensitivity analysis of the effects of reactive uptake coefficients of Cl-OVOCs on simulated chloroacetic acid levels using our updated model was also conducted (Fig. S12). Results show that a change of 1 standard deviation ($\lg \gamma \pm \text{SD}$) in the predicted reactive uptake coefficients for Cl-OVOCs results in either a 5 % increase or an 11 % decrease in the simulated peak of chloroacetic acid. Our study underscores the significance of heterogeneous reactions in the production of chloroacetic acid and other organic acids, highlighting the necessity for more precise reaction parameters in future research.

With the aforementioned updates, the box model significantly improved its ability to simulate chloroacetic acid.

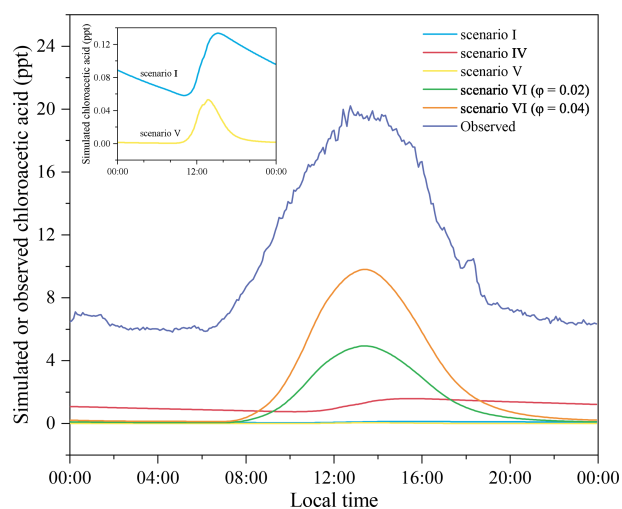


Figure 8. Comparison of measured and simulated diurnal profiles of chloroacetic acid.

However, there is still a discrepancy between the updated simulations and field measurements, which may result from the uncertainty in the parameters we use and other factors affecting chloroacetic acid. For example, previous studies have reported the RH dependence of the reactive uptake coefficients of aldehydes and organic acids (Chen et al., 2021; De Haan et al., 2018; Gen et al., 2018; Tong et al., 2010; Zeineddine et al., 2023). Other reactions of aldehydes in aerosols such as $\cdot\text{OH}$ oxidation, sulfite addition, and Maillard-like reactions with reduced nitrogen species could compete with hydrolysis (Shen et al., 2024; Tang et al., 2022), potentially suppressing the yield of organic acids from the multiphase conversion of aldehydes. α -Chloro- β -ketones such as chloroacetone may also contribute to chloroacetic acid formation through atmospheric heterogeneous chemistry, supported by our QC calculations. In addition to alkenes, other VOCs of high molecular weight, such as ethylbenzene, may serve as precursors of chloroacetic acid (Cui et al., 2021). Moreover, chloroacetic acid may be produced as a disinfection byproduct from the chlorination of dissolved organic matter in the aqueous phase (Jahn et al., 2024).

4 Conclusion

A strong diel pattern of chloroacetic acid was observed at a coastal site in southern China during two photochemically active periods, indicating the intense Cl^{\bullet} -initiated oxidation of VOCs. Chemical box model simulations based on the MCM indicated that ethene, previously proposed as a precursor of chloroacetic acid, contributed less than 1 % to the observed chloroacetic acid concentration. Even when considering other alkenes, their combined contribution would still only be 8 % of the observed value, whereas the model predicts elevated levels of Cl-OVOCs. We conclude that the un-

derestimation of chloroacetic acid and overestimation of Cl-OVOCs can be attributed to the neglect of the heterogeneous processes involving Cl-OVOCs, as indicated by QC calculations. QC calculations reveal the feasibility of the multiphase conversion of chloroacetaldehyde to chloroacetic acid, and the reactive uptake coefficients of Cl-OVOCs including chloroacetaldehyde are estimated to be 3.63×10^{-5} to 2.34×10^{-2} . Adding the heterogeneous processes of these Cl-OVOCs to the MCM model explains 24 %–48 % of the observed chloroacetic acid and exhibits a diurnal pattern similar to the observations, reducing the gaps between observed and simulated results. Future experimental studies are needed to validate the proposed multiphase chemical processes for Cl-OVOCs and establish a reliable yield of chloroacetic acid. In addition, it is important to investigate the implications of OVOC uptake for the fate of these compounds and the subsequent effects on secondary organic aerosols.

Data availability. All of the data used to produce this paper can be obtained by contacting Tao Wang (two.wang@polyu.edu.hk).

Supplement. The supplement related to this article is available online at <https://doi.org/10.5194/acp-25-3753-2025-supplement>.

Author contributions. TW designed the field campaign and data analysis. ML conducted data analysis. MX and YJ conducted the field campaign. ML and TW prepared the manuscript with contributions from all co-authors.

Competing interests. At least one of the (co-)authors is a member of the editorial board of *Atmospheric Chemistry and Physics*. The peer-review process was guided by an independent editor, and the authors also have no other competing interests to declare.

Disclaimer. Publisher's note: Copernicus Publications remains neutral with regard to jurisdictional claims made in the text, published maps, institutional affiliations, or any other geographical representation in this paper. While Copernicus Publications makes every effort to include appropriate place names, the final responsibility lies with the authors.

Acknowledgements. We are grateful to the Hong Kong Environmental Protection Department for providing the sampling locations and access to the VOC and trace gas data, to the Hong Kong Observatory for supplying the meteorological data, and to the Hong Kong Polytechnic University Research Facility in Chemical and Environmental Analysis for providing the ToF-CIMS. We are also very grateful to Qi Yuan for providing part of the VOC data and Fangfang Ma for revising our manuscript.

Financial support. This research is supported by the Hong Kong Research Grants Council (RGC) (project nos. T24-504/17-N and 15217922 to Tao Wang) and the PolyU Distinguished Postdoctoral Fellowship Scheme (grant no. P0039190 to Chunshui Lin).

Review statement. This paper was edited by Qi Chen and reviewed by two anonymous referees.

References

- Blanco, M. B., Bejan, I., Barnes, I., Wiesen, P., and Teruel, M. A.: FTIR product distribution study of the Cl and OH initiated degradation of methyl acrylate at atmospheric pressure, *Environ. Sci. Technol.*, 44, 7031–7036, <https://doi.org/10.1021/es101831r>, 2010.
- Canosa-Mas, C. E., Cotter, E. S. N., Duffy, J., Thompson, K. C., and Wayne, R. P.: The reactions of atomic chlorine with acrolein, methacrolein and methyl vinyl ketone, *Phys. Chem. Chem. Phys.*, 3, 3075–3084, <https://doi.org/10.1039/b101434j>, 2001.
- Cao, X., Gu, D., Li, X., Leung, K. F., Sun, H., Mai, Y., Chan, W. M., and Liang, Z.: Characteristics and source origin analysis of halogenated hydrocarbons in Hong Kong, *Sci. Total Environ.*, 862, 160504, <https://doi.org/10.1016/j.scitotenv.2022.160504>, 2023.
- Carlton, A. G., Turpin, B. J., Altieri, K. E., Seitzinger, S., Reff, A., Lim, H.-J., and Ervens, B.: Atmospheric oxalic acid and SOA production from glyoxal: Results of aqueous photooxidation experiments, *Atmos. Environ.*, 41, 7588–7602, <https://doi.org/10.1016/j.atmosenv.2007.05.035>, 2007.
- Chen, X., Zhang, Y., Zhao, J., Liu, Y., Shen, C., Wu, L., Wang, X., Fan, Q., Zhou, S., and Hang, J.: Regional modeling of secondary organic aerosol formation over eastern China: The impact of uptake coefficients of dicarbonyls and semivolatile process of primary organic aerosol, *Sci. Total Environ.*, 793, 148176, <https://doi.org/10.1016/j.scitotenv.2021.148176>, 2021.
- Choi, M. S., Qiu, X., Zhang, J., Wang, S., Li, X., Sun, Y., Chen, J., and Ying, Q.: Study of Secondary Organic Aerosol Formation from Chlorine Radical-Initiated Oxidation of Volatile Organic Compounds in a Polluted Atmosphere Using a 3D Chemical Transport Model, *Environ. Sci. Technol.*, 54, 13409–13418, <https://doi.org/10.1021/acs.est.0c02958>, 2020.
- Cui, H., Chen, B., Jiang, Y., Tao, Y., Zhu, X., and Cai, Z.: Toxicity of 17 disinfection by-products to different trophic levels of aquatic organisms: Ecological risks and mechanisms, *Environ. Sci. Technol.*, 55, 10534–10541, <https://doi.org/10.1021/acs.est.0c08796>, 2021.
- De Haan, D. O., Jimenez, N. G., De Loera, A., Cazaunau, M., Gratien, A., Pangui, E., and Doussin, J.-F.: Methylglyoxal uptake coefficients on aqueous aerosol surfaces, *J. Phys. Chem. A*, 122, 4854–4860, <https://doi.org/10.1021/acs.jpca.8b00533>, 2018.
- Fang, Y.-G., Tang, B., Yuan, C., Wan, Z., Zhao, L., Zhu, S., Francisco, J. S., Zhu, C., and Fang, W.-H.: Mechanistic insight into the competition between interfacial and bulk reactions in microdroplets through N₂O₅ ammonolysis and hydrolysis, *Nat. Commun.*, 15, 2347, <https://doi.org/10.1038/s41467-024-46674-1>, 2024.
- Franco, B., Blumenstock, T., Cho, C., Clarisse, L., Clerbaux, C., Coheur, P.-F., De Mazière, M., De Smedt, I., Dorn, H.-P., Emmerichs, T., Fuchs, H., Gkatzelis, G., Griffith, D. W. T., Grovov, S., Hannigan, J. W., Hase, F., Hohaus, T., Jones, N., Kerckweg, A., Kiendler-Scharr, A., Lutsch, E., Mahieu, E., Novelli, A., Ortega, I., Paton-Walsh, C., Pommier, M., Pozzer, A., Reimer, D., Rosanka, S., Sander, R., Schneider, M., Strong, K., Tillmann, R., Van Roozendaal, M., Vereecken, L., Vigouroux, C., Wahner, A., and Taraborrelli, D.: Ubiquitous atmospheric production of organic acids mediated by cloud droplets, *Nature*, 593, 233–237, <https://doi.org/10.1038/s41586-021-03462-x>, 2021.
- Frisch, M. J., Trucks, G. W., Schlegel, H. B., Scuseria, G. E., Robb, M. A., Cheeseman, J. R., Scalmani, G., Barone, V., Petersson, G. A., Nakatsuji, H., Li, X., Caricato, M., Marenich, A. V., Bloino, J., Janesko, B. G., Gomperts, R., Mennucci, B., Hratchian, H. P., Ortiz, J. V., Izmaylov, A. F., Sonnenberg, J. L., Williams-Young, D., Ding, F., Lipparini, F., Egidi, F., Goings, J., Peng, B., Petrone, A., Henderson, T., Ranasinghe, D., Zakrzewski, V. G., Gao, J., Rega, N., Zheng, G., Liang, W., Hada, M., Ehara, M., Toyota, K., Fukuda, R., Hasegawa, J., Ishida, M., Nakajima, T., Honda, Y., Kitao, O., Nakai, H., Vreven, T., Throssell, K., Montgomery, Jr., J. A., Peralta, J. E., Ogliaro, F., Bearpark, M. J., Heyd, J. J., Brothers, E. N., Kudin, K. N., Staroverov, V. N., Keith, T. A., Kobayashi, R., Normand, J., Raghavachari, K., Rendell, A. P., Burant, J. C., Iyengar, S. S., Tomasi, J., Cossi, M., Millam, J. M., Klene, M., Adamo, C., Cammi, R., Ochterski, J. W., Martin, R. L., Morokuma, K., Farkas, O., and Foresman, J. B.: Gaussian 16, Revision C.01, 2019.
- Gen, M., Huang, D. D., and Chan, C. K.: Reactive uptake of glyoxal by ammonium-containing salt particles as a function of relative humidity, *Environ. Sci. Technol.*, 52, 6903–6911, <https://doi.org/10.1021/acs.est.8b00606>, 2018.
- Iraci, L. T. and Tolbert, M. A.: Heterogeneous interaction of formaldehyde with cold sulfuric acid: Implications for the upper troposphere and lower stratosphere, *J. Geophys. Res.*, 102, 16099–16107, <https://doi.org/10.1029/97JD01259>, 1997.
- Jahn, L. G., McPherson, K. N., and Hildebrandt Ruiz, L.: Effects of relative humidity and photoaging on the formation, composition, and aging of ethylbenzene SOA: Insights from chamber experiments on chlorine radical-initiated oxidation of ethylbenzene, *ACS Earth Space Chem.*, 8, 675–688, <https://doi.org/10.1021/acsearthspacechem.3c00279>, 2024.
- Jenkin, M. E., Saunders, S. M., and Pilling, M. J.: The tropospheric degradation of volatile organic compounds: a protocol for mechanism development, *Atmos. Environ.*, 31, 81–104, [https://doi.org/10.1016/S1352-2310\(96\)00105-7](https://doi.org/10.1016/S1352-2310(96)00105-7), 1997.
- Jenkin, M. E., Young, J. C., and Rickard, A. R.: The MCM v3.3.1 degradation scheme for isoprene, *Atmos. Chem. Phys.*, 15, 11433–11459, <https://doi.org/10.5194/acp-15-11433-2015>, 2015.
- Jiang, Y., Xia, M., Wang, Z., Zheng, P., Chen, Y., and Wang, T.: Photochemical ageing of aerosols contributes significantly to the production of atmospheric formic acid, *Atmos. Chem. Phys.*, 23, 14813–14828, <https://doi.org/10.5194/acp-23-14813-2023>, 2023.
- Kaiser, E. W., Pala, I. R., and Wallington, T. J.: Kinetics and mechanism of the reaction of methacrolein with chlorine atoms in 1–950 Torr of N₂ or N₂/O₂ diluent at 297 K, *J. Phys. Chem. A*, 114, 6850–6860, <https://doi.org/10.1021/jp103317c>, 2010.

- Lawler, M. J., Sander, R., Carpenter, L. J., Lee, J. D., von Glasow, R., Sommariva, R., and Saltzman, E. S.: HOCl and Cl₂ observations in marine air, *Atmos. Chem. Phys.*, 11, 7617–7628, <https://doi.org/10.5194/acp-11-7617-2011>, 2011.
- Le Breton, M., Hallquist, Å. M., Pathak, R. K., Simpson, D., Wang, Y., Johansson, J., Zheng, J., Yang, Y., Shang, D., Wang, H., Liu, Q., Chan, C., Wang, T., Bannan, T. J., Priestley, M., Percival, C. J., Shallcross, D. E., Lu, K., Guo, S., Hu, M., and Hallquist, M.: Chlorine oxidation of VOCs at a semi-rural site in Beijing: significant chlorine liberation from ClNO₂ and subsequent gas- and particle-phase Cl–VOC production, *Atmos. Chem. Phys.*, 18, 13013–13030, <https://doi.org/10.5194/acp-18-13013-2018>, 2018.
- Lee, B. H., Lopez-Hilfiker, F. D., Mohr, C., Kurtén, T., Worsnop, D. R., and Thornton, J. A.: An iodide-adduct high-resolution time-of-flight chemical-ionization mass spectrometer: Application to atmospheric inorganic and organic compounds, *Environ. Sci. Technol.*, 48, 6309–6317, <https://doi.org/10.1021/es500362a>, 2014.
- Liggio, J., Li, S., and McLaren, R.: Reactive uptake of glyoxal by particulate matter, *J. Geophys. Res.*, 110, 2004JD005113, <https://doi.org/10.1029/2004JD005113>, 2005.
- Ma, F., Ding, Z., Elm, J., Xie, H.-B., Yu, Q., Liu, C., Li, C., Fu, Z., Zhang, L., and Chen, J.: Atmospheric oxidation of piperazine initiated by •Cl: Unexpected high nitrosamine yield, *Environ. Sci. Technol.*, 52, 9801–9809, <https://doi.org/10.1021/acs.est.8b02510>, 2018.
- Ma, F., Xie, H.-B., Li, M., Wang, S., Zhang, R., and Chen, J.: Autoxidation mechanism for atmospheric oxidation of tertiary amines: Implications for secondary organic aerosol formation, *Chemosphere*, 273, 129207, <https://doi.org/10.1016/j.chemosphere.2020.129207>, 2021.
- Ma, W., Chen, X., Xia, M., Liu, Y., Wang, Y., Zhang, Y., Zheng, F., Zhan, J., Hua, C., Wang, Z., Wang, W., Fu, P., Kulmala, M., and Liu, Y.: Reactive chlorine species advancing the atmospheric oxidation capacities of inland urban environments, *Environ. Sci. Technol.*, 57, 14638–14647, <https://doi.org/10.1021/acs.est.3c05169>, 2023.
- Marenich, A. V., Cramer, C. J., and Truhlar, D. G.: Universal solvation model based on solute electron density and on a continuum model of the solvent defined by the bulk dielectric constant and atomic surface tensions, *J. Phys. Chem. B*, 113, 6378–6396, <https://doi.org/10.1021/jp810292n>, 2009.
- Masoud, C. G., Modi, M., Bhattacharyya, N., Jahn, L. G., McPherson, K. N., Abue, P., Patel, K., Allen, D. T., and Hildebrandt Ruiz, L.: High chlorine concentrations in an unconventional oil and gas development region and impacts on atmospheric chemistry, *Environ. Sci. Technol.*, 57, 15454–15464, <https://doi.org/10.1021/acs.est.3c04005>, 2023.
- Neese, F.: Software update: The ORCA program system – Version 5.0, *WIREs Comput. Mol. Sci.*, 12, e1606, <https://doi.org/10.1002/wcms.1606>, 2022.
- NIST Chemical Kinetics Database: <https://kinetics.nist.gov/>, last access: 16 May 2024.
- Orlando, J. J., Tyndall, G. S., Apel, E. C., Riemer, D. D., and Paulson, S. E.: Rate coefficients and mechanisms of the reaction of Cl-atoms with a series of unsaturated hydrocarbons under atmospheric conditions, *Int. J. Chem. Kinet.*, 35, 334–353, <https://doi.org/10.1002/kin.10135>, 2003.
- Osthoff, H. D., Roberts, J. M., Ravishankara, A. R., Williams, E. J., Lerner, B. M., Sommariva, R., Bates, T. S., Coffman, D., Quinn, P. K., Dibb, J. E., Stark, H., Burkholder, J. B., Talukdar, R. K., Meagher, J., Fehsenfeld, F. C., and Brown, S. S.: High levels of nitryl chloride in the polluted subtropical marine boundary layer, *Nat. Geosci.*, 1, 324–328, <https://doi.org/10.1038/ngeo177>, 2008.
- Peng, X., Wang, W., Xia, M., Chen, H., Ravishankara, A. R., Li, Q., Saiz-Lopez, A., Liu, P., Zhang, F., Zhang, C., Xue, L., Wang, X., George, C., Wang, J., Mu, Y., Chen, J., and Wang, T.: An unexpected large continental source of reactive bromine and chlorine with significant impact on wintertime air quality, *Natl. Sci. Rev.*, 8, nwa304, <https://doi.org/10.1093/nsr/nwa304>, 2021.
- Peng, X., Wang, T., Wang, W., Ravishankara, A. R., George, C., Xia, M., Cai, M., Li, Q., Salvador, C. M., Lau, C., Lyu, X., Poon, C. N., Mellouki, A., Mu, Y., Hallquist, M., Saiz-Lopez, A., Guo, H., Herrmann, H., Yu, C., Dai, J., Wang, Y., Wang, X., Yu, A., Leung, K., Lee, S., and Chen, J.: Photodissociation of particulate nitrate as a source of daytime tropospheric Cl₂, *Nat. Commun.*, 13, 939, <https://doi.org/10.1038/s41467-022-28383-9>, 2022.
- Priestley, M., le Breton, M., Bannan, T. J., Worrall, S. D., Bacak, A., Smedley, A. R. D., Reyes-Villegas, E., Mehra, A., Allan, J., Webb, A. R., Shallcross, D. E., Coe, H., and Percival, C. J.: Observations of organic and inorganic chlorinated compounds and their contribution to chlorine radical concentrations in an urban environment in northern Europe during the wintertime, *Atmos. Chem. Phys.*, 18, 13481–13493, <https://doi.org/10.5194/acp-18-13481-2018>, 2018.
- Rodríguez, A., Rodríguez, D., Soto, A., Bravo, I., Diaz-de-Mera, Y., Notario, A., and Aranda, A.: Products and mechanism of the reaction of Cl atoms with unsaturated alcohols, *Atmos. Environ.*, 50, 214–224, <https://doi.org/10.1016/j.atmosenv.2011.12.030>, 2012.
- Saiz-Lopez, A., Fernandez, R. P., Li, Q., Cuevas, C. A., Fu, X., Kinison, D. E., Tilmes, S., Mahajan, A. S., Gómez Martín, J. C., Iglesias-Suarez, F., Hossaini, R., Plane, J. M. C., Myhre, G., and Lamarque, J.-F.: Natural short-lived halogens exert an indirect cooling effect on climate, *Nature*, 618, 967–973, <https://doi.org/10.1038/s41586-023-06119-z>, 2023.
- Saunders, S. M., Jenkin, M. E., Derwent, R. G., and Pilling, M. J.: Protocol for the development of the Master Chemical Mechanism, MCM v3 (Part A): tropospheric degradation of non-aromatic volatile organic compounds, *Atmos. Chem. Phys.*, 3, 161–180, <https://doi.org/10.5194/acp-3-161-2003>, 2003.
- Schütze, M. and Herrmann, H.: Uptake of acetone, 2-butanone, 2,3-butanedione and 2-oxopropanal on a water surface, *Phys. Chem. Chem. Phys.*, 6, 965–971, <https://doi.org/10.1039/B313474A>, 2004.
- Shen, H., Huang, L., Qian, X., Qin, X., and Chen, Z.: Positive feedback between partitioning of carbonyl compounds and particulate sulfur formation during haze episodes, *Environ. Sci. Technol.*, 58, 21286–21294, <https://doi.org/10.1021/acs.est.4c07278>, 2024.
- Simpson, W. R., Brown, S. S., Saiz-Lopez, A., Thornton, J. A., and Von Glasow, R.: Tropospheric halogen chemistry: Sources, cycling, and impacts, *Chem. Rev.*, 115, 4035–4062, <https://doi.org/10.1021/cr5006638>, 2015.

- Soni, M., Sander, R., Sahu, L. K., Taraborrelli, D., Liu, P., Patel, A., Girach, I. A., Pozzer, A., Gunthe, S. S., and Ojha, N.: Comprehensive multiphase chlorine chemistry in the box model CAABA/MECCA: implications for atmospheric oxidative capacity, *Atmos. Chem. Phys.*, 23, 15165–15180, <https://doi.org/10.5194/acp-23-15165-2023>, 2023.
- Spicer, C. W., Chapman, E. G., Finlayson-Pitts, B. J., Platt, R. A., Hubbe, J. M., Fast, J. D., and Berkowitz, C. M.: Unexpectedly high concentrations of molecular chlorine in coastal air, *Nature*, 394, 353–356, <https://doi.org/10.1038/28584>, 1998.
- Tang, S., Li, F., Lv, J., Liu, L., Wu, G., Wang, Y., Yu, W., Wang, Y., and Jiang, G.: Unexpected molecular diversity of brown carbon formed by Maillard-like reactions in aqueous aerosols, *Chem. Sci.*, 13, 8401–8411, <https://doi.org/10.1039/D2SC02857C>, 2022.
- Tentscher, P. R., Lee, M., and von Gunten, U.: Micropollutant oxidation studied by quantum chemical computations: Methodology and applications to thermodynamics, kinetics, and reaction mechanisms, *Accounts Chem. Res.*, 52, 605–614, <https://doi.org/10.1021/acs.accounts.8b00610>, 2019.
- Tong, S. R., Wu, L. Y., Ge, M. F., Wang, W. G., and Pu, Z. F.: Heterogeneous chemistry of monocarboxylic acids on α -Al₂O₃ at different relative humidities, *Atmos. Chem. Phys.*, 10, 7561–7574, <https://doi.org/10.5194/acp-10-7561-2010>, 2010.
- Vijayakumar, S.: Atmospheric fate of formyl chloride and mechanisms of the gas-phase reactions with OH radicals and Cl atoms, *Chem. Phys. Lett.*, 777, 138709, <https://doi.org/10.1016/j.cplett.2021.138709>, 2021.
- Wang, C., Liggio, J., Wentzell, J. J. B., Jorga, S., Folkeron, A., and Abbatt, J. P. D.: Chloramines as an important photochemical source of chlorine atoms in the urban atmosphere, *P. Natl. Acad. Sci. USA*, 120, e2220889120, <https://doi.org/10.1073/pnas.2220889120>, 2023.
- Wang, J., Zhou, L., Wang, W., and Ge, M.: Gas-phase reaction of two unsaturated ketones with atomic Cl and O₃: kinetics and products, *Phys. Chem. Chem. Phys.*, 17, 12000–12012, <https://doi.org/10.1039/C4CP05461J>, 2015.
- Wang, W. and Finlayson-Pitts, B. J.: Unique markers of chlorine atom chemistry in coastal urban areas: The reaction with 1,3-butadiene in air at room temperature, *J. Geophys. Res.*, 106, 4939–4958, <https://doi.org/10.1029/2000JD900683>, 2001.
- Wang, Y., Zhou, L., Wang, W., and Ge, M.: Heterogeneous uptake of formic acid and acetic acid on mineral dust and coal fly ash, *ACS Earth Space Chem.*, 4, 202–210, <https://doi.org/10.1021/acsearthspacechem.9b00263>, 2020.
- Wennberg, P. O., Bates, K. H., Crouse, J. D., Dodson, L. G., McVay, R. C., Mertens, L. A., Nguyen, T. B., Praske, E., Schwantes, R. H., Smarte, M. D., St Clair, J. M., Teng, A. P., Zhang, X., and Seinfeld, J. H.: Gas-phase reactions of isoprene and its major oxidation products, *Chem. Rev.*, 118, 3337–3390, <https://doi.org/10.1021/acs.chemrev.7b00439>, 2018.
- Wolfe, G. M., Marvin, M. R., Roberts, S. J., Travis, K. R., and Liao, J.: The Framework for 0-D Atmospheric Modeling (F0AM) v3.1, *Geosci. Model Dev.*, 9, 3309–3319, <https://doi.org/10.5194/gmd-9-3309-2016>, 2016.
- Xia, M., Wang, T., Wang, Z., Chen, Y., Peng, X., Huo, Y., Wang, W., Yuan, Q., Jiang, Y., Guo, H., Lau, C., Leung, K., Yu, A., and Lee, S.: Pollution-derived Br₂ boosts oxidation power of the coastal atmosphere, *Environ. Sci. Technol.*, 56, 12055–12065, <https://doi.org/10.1021/acs.est.2c02434>, 2022.
- Xue, J., Ma, F., Elm, J., Chen, J., and Xie, H.-B.: Atmospheric oxidation mechanism and kinetics of indole initiated by •OH and •Cl: A computational study, *Atmos. Chem. Phys.*, 22, 11543–11555, <https://doi.org/10.5194/acp-22-11543-2022>, 2022.
- Xue, L. K., Saunders, S. M., Wang, T., Gao, R., Wang, X. F., Zhang, Q. Z., and Wang, W. X.: Development of a chlorine chemistry module for the Master Chemical Mechanism, *Geosci. Model Dev.*, 8, 3151–3162, <https://doi.org/10.5194/gmd-8-3151-2015>, 2015.
- Yang, X.: Reactive aldehyde chemistry explains the missing source of hydroxyl radicals, *Nat. Commun.*, 15, 1648, <https://doi.org/10.1038/s41467-024-45885-w>, 2024.
- Yu, H., Ren, L., Huang, X., Xie, M., He, J., and Xiao, H.: Iodine speciation and size distribution in ambient aerosols at a coastal new particle formation hotspot in China, *Atmos. Chem. Phys.*, 19, 4025–4039, <https://doi.org/10.5194/acp-19-4025-2019>, 2019.
- Zeineddine, M. N., Urupina, D., Romanias, M. N., Riffault, V., and Thevenet, F.: Uptake and reactivity of acetic acid on Gobi dust and mineral surrogates: A source of oxygenated volatile organic compounds in the atmosphere?, *Atmos. Environ.*, 294, 119509, <https://doi.org/10.1016/j.atmosenv.2022.119509>, 2023.
- Zeng, L., Dang, J., Guo, H., Lyu, X., Simpson, I. J., Meinardi, S., Wang, Y., Zhang, L., and Blake, D. R.: Long-term temporal variations and source changes of halocarbons in the Greater Pearl River Delta region, China, *Atmos. Environ.*, 234, 117550, <https://doi.org/10.1016/j.atmosenv.2020.117550>, 2020.
- Zhang, L., Truhlar, D. G., and Sun, S.: Association of Cl with C₂H₂ by unified variable-reaction-coordinate and reaction-path variational transition-state theory, *P. Natl. Acad. Sci. USA*, 117, 5610–5616, <https://doi.org/10.1073/pnas.1920018117>, 2020.
- Zhao, Y. and Truhlar, D. G.: Density functionals with broad applicability in chemistry, *Accounts Chem. Res.*, 41, 157–167, <https://doi.org/10.1021/ar700111a>, 2008a.
- Zhao, Y. and Truhlar, D. G.: The M06 suite of density functionals for main group thermochemistry, thermochemical kinetics, noncovalent interactions, excited states, and transition elements: Two new functionals and systematic testing of four M06-class functionals and 12 other functionals, *Theor. Chem. Acc.*, 120, 215–241, <https://doi.org/10.1007/s00214-007-0310-x>, 2008b.